Summary

Ozone depletion enhanced by volcanism is a primary cause of global warming
Peter L. Ward

Earth is warmed predominantly by visible light from the sun, whereas Earth's atmosphere is warmed primarily by invisible, solar, ultraviolet radiation containing sufficient energy to cause photodissociation of oxygen and ozone. When trace amounts of ozone are depleted, some atmospheric warming is transferred to Earth. Global warming has been greatest in regions where and when ozone depletion was greatest. Anthropogenic chlorofluorocarbons depleted ozone 3% over thirty years while the 1991 eruption of Pinatubo volcano depleted ozone an additional 6% within one year. Large explosive volcanic eruptions also form sulfuric-acid aerosols in the lower stratosphere that reflect, scatter and absorb solar radiation, causing net cooling. But small, effusive, basaltic eruptions deplete ozone substantially without forming significant aerosols, causing net warming. Anthropogenic ozone depletion compounded by eruptions of Icelandic, basaltic volcanoes Eyjafjallajökull (2010) and Grímsvötn (2011) depleted ozone 14% above Toronto, playing a major role in abnormal warming and drought during 2011-2012.

Ozone depletion enhanced by volcanism is a primary cause of global warming

Peter L. Ward[1]

[1] U.S. Geological Survey, retired, Teton Tectonics, P.O. Box 4875, Jackson, WY 83001, USA.

Greenhouse gas concentrations are essentially homogeneous around the globe and have been increasing monotonically over many decades. Greenhouse-gas theory, therefore, cannot explain well-observed decadal to yearly changes in climate within specific geographic regions or more frequent changes in weather without appealing to short-term instabilities in oceanic and atmospheric currents and many other complexities within the climate system. The detailed links between gas concentrations and climate change and between climate change and weather are not clear.

Earth is warmed fundamentally by radiant energy from the sun filtered by the atmospheric ozone column, which can vary more than 10% within hours at mid-latitudes[1] and as much as 50% seasonally in polar regions. Global warming is well-observed to be greatest when and where ozone depletion is greatest[2,3]. Ozone depletion allows solar ultraviolet energy that normally warms the stratosphere to penetrate toward Earth's surface, cooling the stratosphere, warming the troposphere and warming Earth. Anthropogenic chlorofluorocarbons depleted total column ozone 3% over thirty years while the 1991 eruption of Pinatubo volcano depleted ozone an additional 6% within one year. Large explosive volcanic eruptions also form sulfuric-acid aerosols in the lower stratosphere that reflect, scatter, and absorb solar radiation, causing net cooling. But small, effusive, basaltic eruptions deplete ozone substantially without forming significant aerosols, causing net warming. Ozone records from Toronto, Canada, show that anthropogenic ozone depletion compounded by eruptions of Icelandic, basaltic volcanoes Eyjafjallajökull in 2010 and Grímsvötn in 2011 is contemporaneous with and a likely cause of abnormal warming and drought during 2011-2012.

Most solar radiation passes through the atmosphere to heat Earth's surface. Earth loses this heat by conduction, evaporation, convection, and radiation as temperatures fall an average of 6.4°C for each kilometer of increasing altitude throughout the troposphere (Fig. 1). The troposphere is thus heated from below. The stratosphere, on the other hand, is heated from above primarily by solar ultraviolet radiation containing sufficient energy to photodissociate molecular oxygen (O_2) into two atomic oxygen atoms (O) that recombine with O_2 to form ozone (O_3).

Photodissociation is the most effective way to convert electromagnetic radiation into temperature because all of the oscillatory kinetic energy absorbed to break a molecular bond is converted into translational kinetic energy of the two separating atoms or molecules and, according to the kinetic theory of gases, the temperature of a gas is equal to the average translational kinetic energy of all of its atoms and molecules times a constant. The minimum amount of energy required to photodissociate O_2 is nominally 5.11 eV (electronvolts). Since, according to Planck's postulate, energy (E) in an electromagnetic field equals Planck's constant times the frequency of the radiation, only solar radiation containing wavelengths (λ) less than 242.4 nm (nanometers) can provide enough energy to photodissociate O_2.

The highest-energy components of ultraviolet solar radiation are absorbed (filtered out) near the top of the atmosphere. Lower and lower energy components are filtered out progressively closer and closer to earth. The thermal structure of the atmosphere is a dynamic balance primarily between the highest energy solar radiation to penetrate to a given altitude, i.e. the amount of energy that one molecule can absorb, the concentration of molecules that can absorb it, and the rapid increase in

2

density (black line, Fig. 1, logarithmic scale), i.e. the number of molecules whose translational kinetic energy must be increased to raise the temperature. Modern chemical-transport climate models include more than 45 photodissociation reactions and more than 100 gas-phase chemical reactions[4], but the most important for warming center around nitrogen, making up 78% of the volume of the atmosphere, oxygen (21%), and ozone (<0.0015%). The very small amounts of ozone are important because the photodissociation of ozone and its recombination are catalytic processes that typically occur over and over, converting electromagnetic energy into temperature while not necessarily changing the amount of ozone.

The small amount of solar radiation in the extreme ultraviolet (λ<124 nm, E>10.0 eV) is absorbed above an altitude of ~85 km primarily through photoionization of N_2, O_2, and NO. CO_2 is photodissociated when λ<167 nm (E>7.4 eV); SO_2 when λ<200 nm (E>6.2 eV).

The greatest heating of the Earth/atmosphere system occurs all day, every day at the stratopause near 50 km altitude where the temperature is maintained typically 55°C warmer than the temperature at the tropopause. The stratopause if formed at an altitude where there are sufficient O_2 molecules at sufficiently low enough atmospheric densities being dissociated by sufficiently energetic ultraviolet radiation to cause the maximum increase in temperature. At decreasing altitudes in the stratosphere, lower and lower energy radiation is still available, so that even though there are rapidly increasing numbers of atoms and molecules, their mean translational velocities decrease, limiting the temperature increase.

The tropopause is the boundary between the troposphere heated from below and the stratosphere heated from above. It also forms a boundary between low ozone mixing ratios in the troposphere and high ozone mixing ratios in the stratosphere especially between 14 and 32 km (Fig. 1). The troposphere contains <10% of total column ozone[1]. The average height of the tropopause varies from 16.6 km near the equator where solar radiation is most intense to 9 km near the poles[5]. Annual mean heights increased ~160 m between 1980 and 2004 while the lower stratosphere cooled ~2°C, the upper troposphere warmed[5] ~0.1^{o}C and mean surface temperatures in the northern hemisphere[6] rose ~0.5^{o}C.

But the tropopause is a very dynamic boundary. On June 19, 2004, for example, the height of the tropopause above Montreal, Canada, dropped from 13.5 km to 8.5 km in 5 hours at the same time that total column ozone increased 20% (70 DU, Dobson Units)[1]. "From the time of Dobson's early measurements" in the 1920s, "it has been known that the total ozone amount undergoes large day-to-day fluctuations"[7] in the mid to high latitudes where the Brewer-Dobson circulation brings stratospheric ozone formed mostly in the tropics down into the lower stratosphere and upper troposphere. Averages of these large changes are now mapped daily throughout the world as observed from satellites and ground stations[8] (Fig. S5 in the Supplementary Information).

Early observations similarly showed "that there is a strong correlation between column ozone and meteorological conditions"[1,7] including atmospheric and surface temperatures and the resulting depth and location of surface pressure highs and lows. These meteorological conditions have traditionally been assumed to cause ozone variations. But ozone depletion allowing more high-energy ultraviolet solar radiation into the lower stratosphere and troposphere and associated exothermic photodissociation provides a clear mechanism to heat the atmosphere differentially across small regions and over timescales of hours to days having a direct impact on weather systems. Long-term changes in ozone are thus highly likely to have a major impact on climate.

The narrow band for photodissociation
The spectrum of radiation available from an overhead sun that normally reaches a given altitude is shown by actinic flux (AF) in Fig. 2. Absorption by the ozone layer is essentially the difference in actinic flux at 40 and 15 km (dashed red and solid purple lines respectively in Figs. 1 and 2).

Tropospheric warming due to photodissociation is confined to a very narrow bandwidth (red shaded area) sandwiched between the very rapidly increasing availability of solar energy with wavelengths >290 nm (red dotted and purple lines) and the rapidly increasing absorptivity of ozone at wavelengths <340 nm (black line).

A 30% decrease in total column ozone will increase UV radiation at Earth's surface 1.02 W m^{-2} for overhead Sun and 0.276 W m^{-2} for a solar zenith angle of 70° (red shaded area)[9]. These changes in energy flux, when integrated over Earth's surface, have the potential to explain at least some and possibly most of the observed warming believed caused by changes of <1 W m^{-2} in the total energy budget of Earth's atmosphere[10].

The primary exothermic photochemical process in the lower stratosphere and down into the troposphere is the photodissociation of O_3 to form O_2 plus an excited oxygen atom, $O(^1D)$, for λ<310 nm (E>4.0 eV). Quantum yields (fraction of molecules dissociated) as large as 0.08 have been observed for λ=330 nm[11]. Matsumi et al.[11] find that "photodissociation from vibrationally excited ozone contributes approximately 25 to 40% to the overall production rate for solar zenith angles from 40° to 80° respectively." Note the increase as ray paths lengthen toward the poles.

Longer wavelengths (463-1180 nm) throughout the range of visible light into the near infrared have sufficient energy to photodissociate ozone into O_2 plus the ground state oxygen atom $O(^3P)$ that reacts with O_2 to form ozone again[11]. The net amount of ozone does not change, but this catalytic reaction continually converts radiant energy into higher velocities of the molecules, increasing temperature. Photodissociation of nitrogen dioxide (NO_2) can similarly produce $O(^3P)$ for λ<397.8 nm but with quantum yields >0.1 for λ<~411 nm[12]. Note in Fig. 2 the sudden decrease in actinic flux at all levels for λ<~411 nm.

Ozone depletion increases the amount of high-energy ultraviolet radiation reaching the lower troposphere to cause photodissociation of O_3 and NO_2, to be absorbed by SO_2, and to be absorbed at Earth's surface. On land, much of the energy absorbed during the day is radiated back into the atmosphere at night. At sea, however, ultraviolet radiation penetrates the ocean to depths >10 meters[13] and is thus more effective at heating the ocean than infrared radiation absorbed near the surface where much of the energy is lost back into the atmosphere at night. The effect of this UV on surface temperatures could be small, while its effect on increasing ocean heat content could be substantial.

Regions and times of greatest warming
The greatest warming observed on Earth between 1976 and 2005, according to the Intergovernmental Panel on Climate Change, was during June through August around the Western Antarctica Peninsula[2] and during December through February in North America, northern Europe and northwestern Russia[3], the times and locations of greatest ozone depletion where there is still sufficient solar flux to cause warming. At Faraday/Vernadsky station on the Antarctic Peninsula (65.4^oS) increases in temperature are strongly correlated with decreases in total column ozone[14]. Minimum monthly temperatures increased 6.7^oC from 1951 to 2003[14], the greatest warming of this region in more than 1800 years[15]. Maximum monthly temperatures and ozone levels changed very little during summer months while summer surface temperatures of the Bellingshausen Sea rose 1^oC[16]. Winter sea ice decreased 10% per decade and shortened in seasonal duration[17]; 87% of marine glaciers in this region retreated, many collapsing into the ocean following the loss of seven very large ice shelves[18]. The Circumpolar Deep Water of the Antarctic Circumpolar Current warmed[17]. Warming of interior Antarctica was slowed by the high mean albedo (~0.86) of Antarctic snow, nearly twice the albedo of Arctic snow[19], and by the increase in solar zenith angle (decrease in solar flux) approaching South Pole.

4

In the Arctic, ozone depletion in early 2011 was unprecedented, exceeding 80% at altitudes of 18-20 km, comparable for the first time with the Antarctic ozone hole[20]. The extent of Arctic sea ice, declining at >11% per decade since 1979[21], reached a record low on September 16, 2012, nearly 50% lower than the average extent between 1979 and 2000[22]. The estimated maximum extent of seasonally frozen ground in the northern hemisphere[23] has decreased ~7% from 1901 to 2002, with the largest changes since 1980.

The greatest global warming observed has been in the regions and at the times of the greatest ozone depletion.

Ozone depletion observed over time

The longest continuous measurements of total column ozone have been made since 1927 at Arosa, Switzerland (black line, Fig. 3). The dashed gray line with blue data markers shows from 1964 to 2009 the annual mean area-weighted total ozone deviation from the 1964-1980 means for northern mid-latitudes (30°N-60°N) scaled from -8% at the bottom of the figure to 10% at the top[24]. Years of increasing or decreasing ozone are nearly identical at Arosa and for this area-weighted mean with small differences in amplitude. Thus the Arosa data provide a reasonable approximation for ozone changes throughout northern mid-latitudes since 1927.

Total column ozone at Arosa averaged around 331 DU until 1974, fell 9.4% to 300 DU by 1993 and began generally rising again until 2011. The long-term decrease in ozone has been reliably associated with an increase in concentrations of anthropogenic chlorine (green line, y-axis inverted) through chlorine catalyzed destruction of ozone[25]. The resulting Montreal Protocol on Substances That Deplete the Ozone Layer was signed beginning in 1987, leading to phasing out the production of chlorofluorocarbons and hydrochlorofluorocarbons and a decrease in tropospheric chlorine beginning in 1993. Long-term ozone concentrations are expected to return to late-1970's levels by 2040[25].

The largest short-term peak in annual mean total column ozone shown in Fig. 3 occurred in 1940-1941, possibly related in some way to the onset of World War II. Large peaks in ozone also occur during years containing the three largest atmospheric nuclear tests labeled in black with yield in megatons. There is a peak in 1998 during one of the largest El Niños in history but no obvious peak in 1982-1983 during an El Niño with a comparably large multivariate ENSO index[26], although the latter observation may have been complicated by the eruption of El Chichón in 1982. But the most consistent short-term changes in ozone in Fig. 3 are an apparent increase in ozone during the year of a volcanic eruption followed by a much larger depletion during the next few years.

The major effects of volcanism on ozone

The largest eruption since 1912 was in 1991 from Pinatubo with a VEI (logarithmic Volcano Explosivity Index) of 6. An even larger ozone anomaly in 2010 is associated with the 100-times smaller basaltic fissure eruption of Eyjafjallajökull in Iceland (VEI=4). A slightly larger VEI=4 eruption of Grímsvötn, 140 km northeast of Eyjafjallajökull, occurred in May, 2011, compounding the amount of ozone depletion during 2011-2012. The amplitudes of these short-term ozone anomalies since 1990 are larger than the amplitudes of earlier volcanic anomalies before the global rise in tropospheric chlorine (green line, y-axis inverted). Anomalies appear associated with the eruption of Hekla in Iceland (1970, VEI=3) and with the larger eruptions of El Chichón in Mexico (1982, VEI=5 and 4+) and Agung in Bali (1963, VEI=5 and 4). Mt. St. Helens in Washington state (1980, VEI=5) had little effect on global temperature or ozone most likely because the main eruption was a blast of steam triggered by a landslide on the intruding volcanic plug[27]. The increase in ozone during the year of each major eruption is discussed in the Supplementary Information.

Depletion of stratospheric ozone during years following a volcanic eruption has been observed widely especially related to Pinatubo[28,29]. By January-April, 1993, total column ozone was 11 to 17% below preceding years throughout Canada with a peak loss of 30% at ~16 km[30]. On average, total ozone decreased 8% in Europe, 5-6% in North America, Russia, and Asia but <2% in the tropics[29]. Following Agung and El Chichón, the deceases were 5%, 2-3%, and <2% in these same regions. Following Pinatubo, lower tropospheric warming of up to 3°C during the winter was observed throughout the more northerly parts of the northern continents[31], the parts with greater depletion of ozone. Related major changes in atmospheric chemistry are well documented by a 45% drop in total column NO_2 above Switzerland beginning five months after the Pinatubo eruption and returning to normal with an e-folding time of two years[32], a 40% decrease in NO_2 column observed above New Zealand[33], and substantial increases in HNO_3 concentrations due to heterogeneous conversion of N_2O_5[34].

The observed ozone depletion (black line, Fig. 3) was accompanied by cooling of the stratosphere (purple line) occurring mostly "as two downward 'steps' coincident with the cessation of transient warming after the major volcanic eruptions of El Chichón and Mount Pinatubo"[35] and a similar downward step following the 1963 eruption of Agung volcano[36].

Ozone depletion following volcanic eruptions has traditionally been explained by new aerosols formed in the lower stratosphere providing substantial new surfaces for heterogeneous chemical reactions to form ozone-destroying chlorine at cold temperatures[37]. Yet water vapor (H_2O), the most voluminous gas erupted from volcanoes, is the primary source of OH radicals that catalytically destroy ozone in the stratosphere[34,38]. Volcanoes also erupt megatons of halogens[34], primarily chlorine and bromine[39] and only one halogen molecule can destroy >100,000 molecules of ozone[40]. During explosive eruptions, many of these halogens appear to be removed immediately from the eruptive cloud in condensed supercooled water[41]. But effusive, basaltic eruptions such as Eyjafjallajökull and Grímsvötn do not form significant eruption columns that remove halogens and that create aerosols in the stratosphere. They typically involve 10-100 times more volatiles per cubic kilometer of magma than explosive eruptions caused by more chemically evolved magmas[42]. Ozone depletion is substantial within the plumes of erupting volcanoes; detailed observations imply that "the most likely cause for the observed rapid and sustained O_3 loss to be catalytic reactions with halogen, mainly bromine, radicals"[43]. Recent field observations have shown that even the plumes of quiescently degassing volcanoes are chemically very active containing halogens that modeling shows cause ozone depletion[44].

Volcanic eruptions are typically followed a year later by ~6% depletion of ozone averaged throughout the year (Fig. 3). How do these short-term effects of volcanism compare to the longer-term effects of anthropogenic chlorofluorocarbons? The green line for chlorine is inverted and has been scaled so that the increase in anthropogenic tropospheric chlorine from 1965 to 1993 has approximately the same rate of change as the corresponding long-term decrease in ozone as expected by current theory. This visual fit suggests that depletion of ozone following the Pinatubo eruption (~20 DU) was twice as large as the depletion due to chlorofluorocarbons since 1960 (~10 DU) and that it takes more than a decade for ozone concentrations to return to pre-eruption levels. Large, explosive volcanic eruptions are well known to form sulfuric acid aerosols in the lower stratosphere that reflect, scatter, and absorb solar radiation, causing cooling at Earth's surface of ~0.5^{o}C over three years. These explosive eruptions also deplete ozone causing warming that lasts 3 to 5 times longer than the aerosols, but the cooling effects of the aerosol predominate. The much less explosive and much more numerous basaltic effusive eruptions such as Eyjafjallajökull and Grímsvötn as well as quiescently degassing volcanoes[44] do not form significant aerosols in the lower stratosphere so that ozone depletion and related warming are dominant.

Warming and drought in 2011-2012

The blue line in Fig. 4a shows the average monthly total column ozone measured above Toronto, Canada, averaged for the years 1961 through 1970 when anthropogenic tropospheric chlorine had only increased 16% from levels in 1925 towards peak levels in 1994 (green line, Fig. 3). The green line in Fig. 4a shows average monthly column ozone for 2009 when anthropogenic chlorine had decreased 9% from its peak value. Note that ozone depletion is greatest between December and May, the months of greatest warming in the northern hemisphere[3]. According to theory, the mean change in radiative forcing between the 1960s and 2009 caused by ozone depletion should be directly proportional to the area between the blue and green lines.

The solid red line includes both the increase in ozone during February preceding the first eruption of Eyjafjallajökull in March, 2010, discussed in the Supplementary Information, and subsequent depletion. The dashed red line shows total ozone in 2011 including depletion due to Eyjafjallajökull and increases and decreases related to the eruption of Grímsvötn. The double red line shows ozone levels in 2012. Note that since November 2011, the times when monthly maximum temperature records have been set throughout central North America[45], ozone has been depleted as much as 14% below mean values in the 1960s.

The dashed black line in Fig. 4b shows the average for each year of the monthly mean total column ozone above Toronto averaged over four consecutive months from December through April; the dashed red line (y-axis inverted) shows the same average for monthly mean minimum temperatures. The solid lines are the same data smoothed using a 3-month symmetric running mean. A substantial decrease in ozone is typically but not always associated with an increase in minimum temperature except in 1992-1995 when aerosols in the lower stratosphere following the June, 1991, eruption of Pinatubo decreased radiation from the Sun as much as 2.7 ± 1.0 W m^{-2} during August and September decaying exponentially to negligible values by 1995[46]. Note the extremely low ozone and high temperature in early 2012 (circled data points, lower right).

These data suggest that depletion of ozone due to the eruption of Eyjafjallajökull in 2010 and Grímsvötn in 2011 supplemented anthropogenic depletion leading to extreme ozone depletion and the resulting extreme temperatures and drought observed throughout central North America during late 2011 and 2012 and the highest sea surface temperatures ever recorded on the continental shelf off the northeastern United States during the first half of 2012[47]. The drought of 2012 approached the intensity of the great Dust Bowl droughts of 1934 and 1936 when a highly unusual sequence of seven VEI 4 and 5 eruptions occurred from 1931 through 1933 in Indonesia, Japan, Kurile Islands, Kamchatka, Alaskan, Guatemala, and Chile[48].

Recent warming and drought might have been enhanced by the fact that November, 2011, had the largest number of sunspots per month since October, 2002[49], and ultraviolet insolation increases four to six times more than broadband irradiance during solar cycles[50]. In 1933 and 1934, however, the numbers of sunspots per month were relatively low until late in 1936.

Photodissociation is required for warming

Annual mean surface temperatures in the northern hemisphere (red line, Fig. 5) increased during the 1930s, cooled during the 1940s, remained relatively constant until 1975, rose rapidly until 1998 with a net temperature increase of ~0.8°C, and have remained relatively constant until 2011[51,52].

Total tropospheric chlorine caused by anthropogenic chlorofluorocarbons (green line) increased rapidly from 1970, reached a peak in 1993 due to implementation of the Montreal Protocol and continues to decline slowly.

Annual mean total column ozone (O_3, black line, y-axis inverted) fell rapidly from 1971 to 1995 and has been recovering slowly until the volcanic eruptions in 2010 and 2011. A slight delay after changes in chlorine concentration is expected since most ozone is formed above the tropics

and moves slowly via Brewer-Dobson circulation to high latitudes where most ozone destruction occurs during winter associated with polar stratospheric clouds.

The primary time delay in the atmospheric system involves the heat capacity of the ocean covering 71% of Earth. The observation in Fig. 5 that ocean surface temperature rose ~5 years after the decrease in ozone is in the range of calculations by Hansen et al.[53] for a 3.5-year e-folding time for warming the ocean if the equilibrium temperature of Earth suddenly increased a small amount and a 10-year e-folding time taking into account an ocean with a 100-meter-thick mixed-layer.

World ocean heat content (dashed purple line) increased from 1970 to 1980, remained relatively constant until 1990, and has been increasing ever since. The time relationship between ocean heat content, volcanism, and annual total ozone is shown more clearly by the dashed red line in Fig. 3 where the ozone data have not been smoothed. The slow change in ocean heat content between 1980 and 1990, smoothed with a 5-year running mean, reflects the observed global cooling of up to $0.5^{o}C$ for up to three years following the eruptions of El Chichón (1982) and Pinatubo (1991)[54]. Continued rise of ocean heat content since 1998 is expected since column ozone has remained depleted.

The annual rate of increase in concentrations of CO_2 (blue line) was <0.1 ppm/yr from 1938 to 1947 but began increasing to 0.7 ppm/yr by 1960 as concentrations of SO_2 and other anthropogenic pollutants (Fig. S3) were rapidly increasing. From 1976, when ocean heat content began increasing, the annual rate of increase of CO_2 doubled and even quadrupled to between 1.3 and 2.7 ppm/yr most likely due to decreasing CO_2 solubility in a warming ocean. Annual CO_2 concentrations increased with industrialization and with ocean temperature, but slowed during the three years following major volcanic eruptions even though CO_2 was the second most voluminous gas erupted after water vapor.

SO_2 emissions (dashed black line), 88% from burning fossil fuels, rose rapidly from 1950 until 1973 when concern over acid rain led to the addition of smokestack-scrubbers and other emission controls, as well as substitution of North Sea oil for coal in Europe. The result was a 20% decrease in SO_2 emissions by 2002. Similar increases were observed in NO_X, methane, and black carbon accompanied by a decrease and then increase in surface solar radiation (Fig. S3).

SO_2 and related pollution increased ~30 years before the major increase in temperature suggesting that major increases in anthropogenic pollution did not affect global temperatures until ozone was depleted. Thus absorption without photodissociation does not appear to cause substantial global warming. Similarly, the observation that the lowest temperatures in the stratosphere are near the base of the ozone layer where ozone concentrations are highest (Fig. 1) implies that simple absorption by ozone is less important for warming the stratosphere than absorption that leads to photodissociation.

What about greenhouse gases?
Concentrations of CO_2 increased monotonically at an accelerating rate since 1998, while mean global temperatures remained relatively constant[51,52]. The sensitivity of climate to a doubling of carbon dioxide has not been observed directly in nature nor in the laboratory but has been estimated by assuming temperature increases over specific time intervals resulted primarily from absorption by greenhouse gases. Yet photodissociation and ozone depletion clearly contribute to warming and absorption without photodissociation may not cause much warming. There are several issues explained in the Supplementary Information that need to be evaluated in the laboratory and in the field before we can determine quantitatively the relative importance of greenhouse gases:
1. Molecules of greenhouse gases are well documented to absorb radiant energy along spectral lines that correspond to combinations of the resonant frequencies of the gas molecule's chemical bonds and rotational degrees of freedom (Figs. S1 and S2). This means that oscillatory kinetic

energy in the radiation field is absorbed as oscillatory kinetic energy within each molecule. But temperature of a gas is proportional to translational kinetic energy. What proportion of the oscillatory kinetic energy is converted to translational kinetic energy during the numerous collisions of gas molecules in the atmosphere?

2. An incandescent light bulb emits a broad spectrum of radiation described by Planck's law for black-body radiation (blue line, Fig. S1) and is perceived as being hot. A fluorescent light bulb emits radiation over very narrow parts of the visible spectrum (black line, Fig. S1) and is perceived as being cool. Over how broad a spectrum does a layer of molecules dispersed in a gas radiate? Is a layer of gas properly described as a black body?

3. Heat in matter flows from warm to cool. If radiation is absorbed via resonance, which it appears to be, heat flows from higher spectral intensity in the radiation field to lower spectral intensity within the molecule. While radiation propagates in all directions, absorption may only occur from higher to lower spectral amplitude; otherwise the radiation is reflected. Our bodies absorb radiant heat, but we do not perceptively absorb radiant cold; instead we lose body heat more efficiently into a cold environment. We sense an ice cube by touch and the flow of heat from our body to the ice cube.

High-resolution paleoclimatic studies in the Late Miocene[55] and the existence of glaciation in Devonian and Permian-Triassic times when CO_2 concentrations were >10 and >5 times preindustrial values respectively[56] question prevailing thoughts that increased concentrations of CO_2 cause global warming. Similarly the width of the tropical belt widened 2° to 5° in latitude since 1979[57]. While expansion in the Southern Hemisphere has been attributed to ozone depletion[58], Allen et al.[59], use the Community Atmosphere Model to suggest that "recent Northern Hemisphere tropical expansion is driven mainly by black carbon and tropospheric ozone, with greenhouse gases playing a smaller part."

Periods of sudden global warming are contemporaneous with major increases in volcanism at the end of the last ice age (Fig. S4), during 13 Dansgaard-Oeschger sudden warming events in the past 46,000 years, during the opening of the North Atlantic in the Early Eocene, and during the 12 largest mass extinctions over the past 360 million years[60] explained in more detail in the Supplementary Information.

Discussion

The temperature of Earth's surface is a very delicate and dynamic balance between solar energy received at the surface and thermal energy flowing away from the surface, but the tropopause forms the physical boundary between the troposphere heated from below by a sun-warmed Earth and the stratosphere heated from above. The height of the tropopause can vary by kilometers within hours and is closely related by observations and theory to total column ozone. More ozone absorbs more solar ultraviolet energy in the stratosphere, warming the stratosphere, lowering the height of the tropopause, and cooling earth. Less ozone allows more ultraviolet energy to reach Earth, cooling the stratosphere, raising the height of the tropopause, and warming Earth. Total column ozone is depleted primarily by chemically active forms of chlorine and bromine emitted by man and by volcanic eruptions. Trace amounts of ozone are so effective because ozone is photodissociated by ultraviolet and visible radiation in cyclic processes that efficiently convert oscillatory energy in radiation into translational kinetic energy (temperature) in the atmosphere. The greatest warming at Earth's surface is in the places and at times of greatest ozone depletion. Widespread observations show the importance of these processes qualitatively. A quantitative proof will only be possible when climate models are adapted to include the many issues raised in this paper and listed at the end of the Supplementary Information.

Supplementary Information is available in the online version of the paper.

Figure Captions
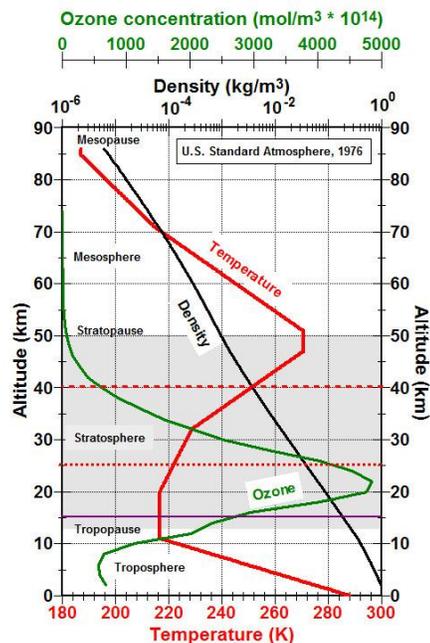
Figure 1 | The greatest warming in the atmosphere is between 35 and 60 km while the greatest concentrations of ozone are between 14 and 32 km. The profiles shown are for the U.S. Standard Atmosphere 1976. Actual profiles vary primarily with latitude, time of day, season and amount of ozone depletion. The dashed and dotted red lines and solid purple line correspond to altitudes of actinic flux calculations in Fig. 2. The sources and units for all data plotted in all figures are listed in the Supplementary Information available in the online version of the paper.
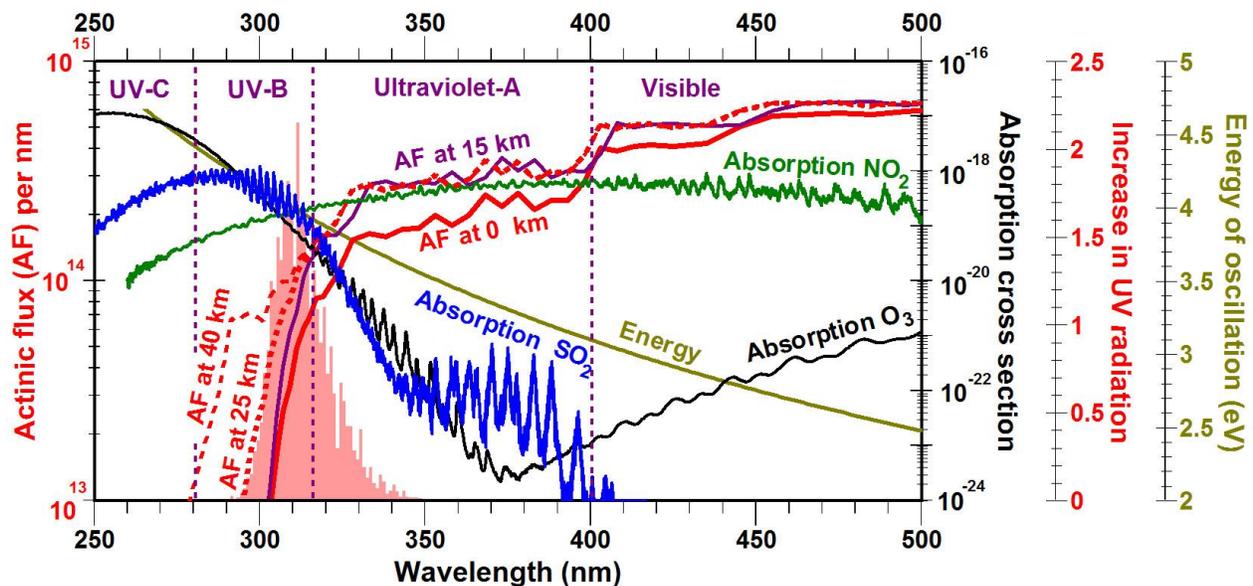
Figure 2 | A 30% decrease in total column ozone increases ultraviolet radiation reaching Earth's surface by ~1.02 W m^{-2} between 290 and 340 nm (red shaded area) when Sun is directly overhead[9]. O_3, SO_2, and NO_2 absorb solar energy strongly at wavelengths <400 nm. Absorption by O_3 and NO_2 typically leads to photodissociation for wavelengths <411 nm.
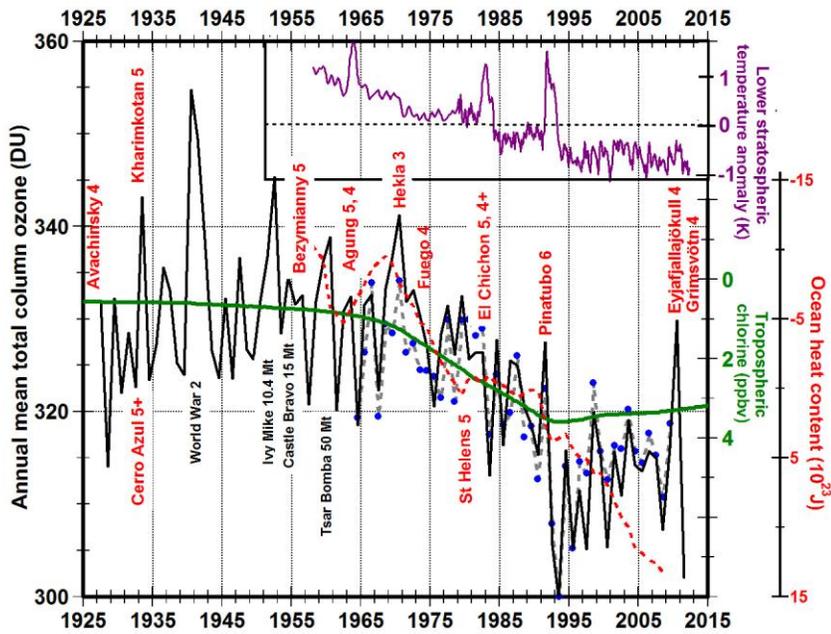
Figure 3 | Total column ozone (black line) peaks during years with major volcanic eruptions and then drops precipitously by more than twice as much during the following year causing a cooling in the lower stratosphere (purple line). The ozone data were measured at Arosa, Switzerland. The names of the erupting volcanoes and the Volcano Explosivity Index (VEI) for each large eruption are labeled in red. The green line shows annual mean tropospheric chlorine with the y-axis inverted. The dashed red line with the y-axis inverted shows the increase of ocean heat content.
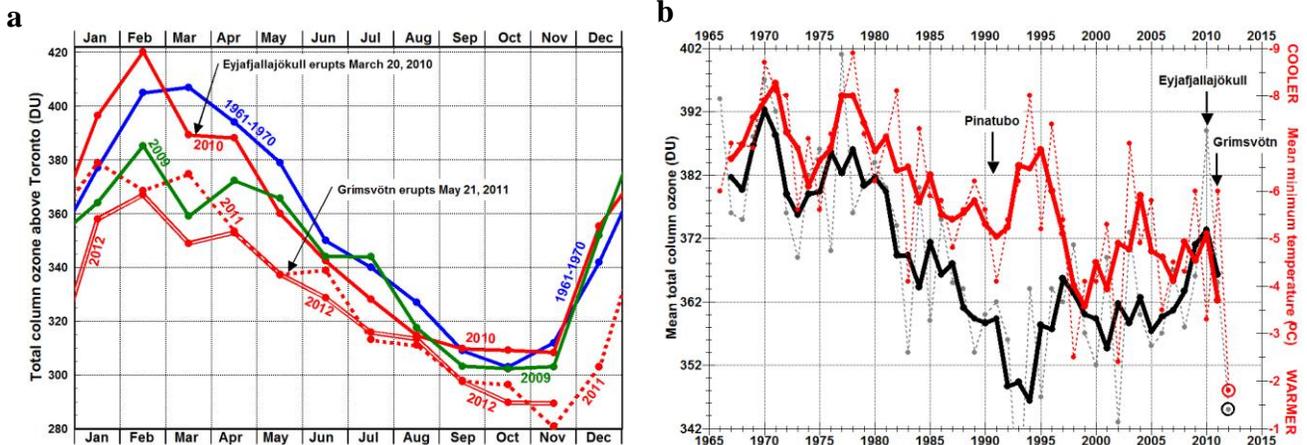
Figure 4 | Ozone reached a minimum in 2012 when temperatures reached a maximum.
a, Total column ozone above Toronto, Canada, in November, 2011, was 12% below the average for Novembers in 1961 through 1970 and has remained unusually low throughout 2012. **b,** When mean total column ozone measured during the months of December through April in Toronto Canada (black line) decreases, mean minimum temperature for the same months typically warms (red lines, y-axis inverted). The dashed lines show annual means; the solid lines are smoothed using a 3-point centered running mean.

12
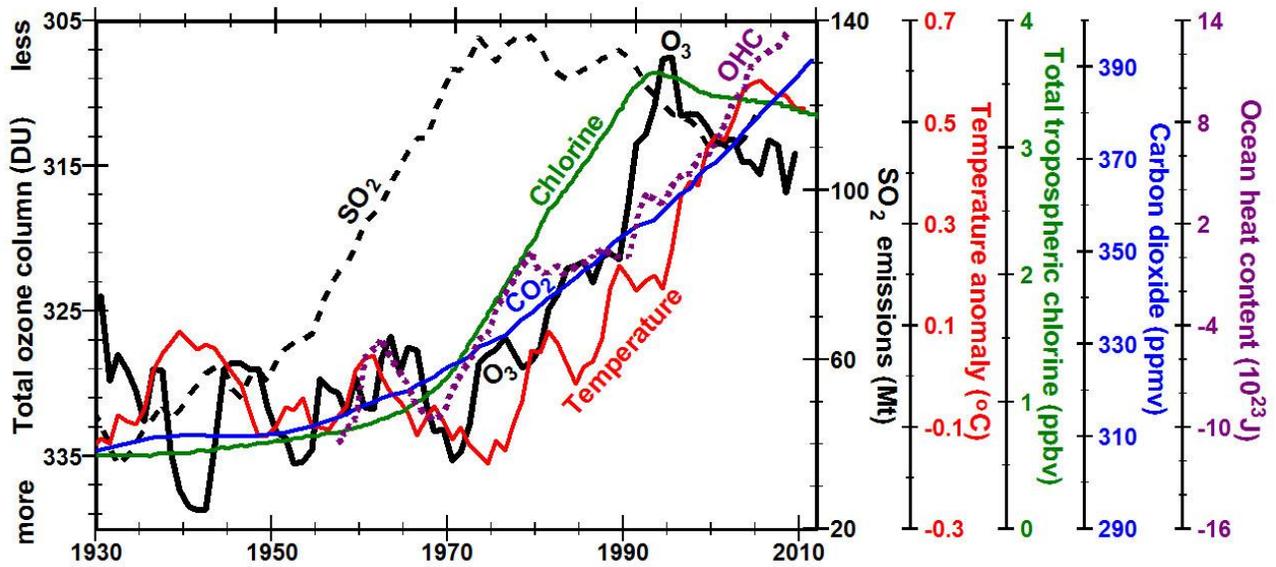
Figure 5 | Increased SO₂ pollution (dashed black line) does not appear to contribute to substantial global warming (red line) until total column ozone decreased (black line, y-axis inverted), most likely due to increasing tropospheric chlorine (green line). Mean annual temperature anomaly in the Northern Hemisphere (red line) and ozone (black line) are smoothed with a centered 5 point running mean.

Supplementary Information

Data Sources

Figure 1 | For the U.S. Standard Atmosphere 1976: red line is temperature[61], black line is density[61], and green line is ozone[62].

Figure 2 | Absorption by nitrogen dioxide (NO_2)(green line)[63], ozone (O_3)(black line)[63], and sulfur dioxide (SO_2)(blue line)[64,65], increase in radiation in response to a 1% decrease in the total column ozone (near 300 DU) (red shaded area)[9], actinic flux (red and purple lines) as estimated by Madronich in Tables 3.7, 3.15, 3.16, 3.17[66], energy of radiation (olive line) based on Planck's postulate where energy equals Planck's constant times frequency. Actinic flux is photons cm^{-2} s^{-1}, absorption cross section is cm^2 per molecule, increase in UV radiation is mW m^{-2} nm^{-1} times 10^5, and energy in electronvolts.

Figure 3 | Annual total column ozone (black line) in Dobson units at Arosa, Switzerland[67], in eastern Switzerland at an elevation 1820 meters is from ftp://iaclin2.ethz.ch/pub_read/maeder/totozone_arosa_yearly. Thanks to Johannes Staehelin and Rene Stuebi for updates. Total tropospheric chlorine (green line) in parts per billion by volume from Plate 6[25], ocean heat content (dashed red line with blue data points) from Fig. 1[68], lower stratospheric temperature anomaly (purple line) based on radiosonde data before 1979[69] and satellite data since[70] smoothed with a seven-month centered running mean, volcanism from http://www.volcano.si.edu/world/largeeruptions.cfm, and nuclear tests from http://en.wikipedia.org/wiki/Nuclear_weapons_testing. The dashed gray line with blue data markers from Fig. 2-2[71] shows from 1964 to 2009 the annual mean area-weighted total ozone deviation from the 1964-1980 means for northern mid-latitudes (30^oN-60^oN) scaled from -8% at the bottom of the figure to 10% at the top.

Figure 4 | Ozone (measured at Environment Canada and the University of Toronto from www.woudc.org/data_e.html. Thanks to Vitali Fioletov and Tom Matthews for access to preliminary ozone data. Temperature (red line) measured at the Toronto Airport by Environment Canada from www.climate.weatheroffice.gc.ca/climateData/dailydata_e.html?StationID=5097.

Figure 5 | Annual total column ozone (black line) in Dobson units at Arosa, Switzerland[67] ftp://iaclin2.ethz.ch/pub_read/maeder/totozone_arosa_yearly, SO_2 emissions (black line)[72], temperature anomaly in reference to the average from 1961-1990 (red line) www.cru.uea.ac.uk/cru/data/temperature/hadcrut3nh.txt, total tropospheric chlorine (green line) in parts per billion by volume from Plate 6[25], CO_2 ftp.cmdl.noaa.gov/ccg/co2/trends/co2_annmean_mlo.txt, and ocean heat content in reference to the average from 1955-2006 (dotted purple line) from Fig. 1[68]. Knight et al.[52] calculate that global temperatures only rose 0.07 ± 0.07^oC from January 1999 through December 2008.

Temperature versus absorption spectra

According to Planck's law, a black body, an idealized perfect absorber and emitter of electromagnetic radiation, radiates the spectral intensity shown by the solid lines in Fig. S1 assuming 5770K as the temperature for Sun and 288K for Earth. The shapes of these lines are similar, but the wavelength of maximum spectral intensity (λ_{max}) decreases with increasing temperature according to Wien's displacement law where λ_{max} in micrometers (μm) (1 μm=1000 nm) equals 2897 divided by temperature in Kelvin or the color temperature max (T_{max}) of EMR at λ_{max} equals 2897 divided by λ_{max}. Since radiation diverges with distance, the dashed red line shows the radiation from the sun at the top of Earth's atmosphere.

14
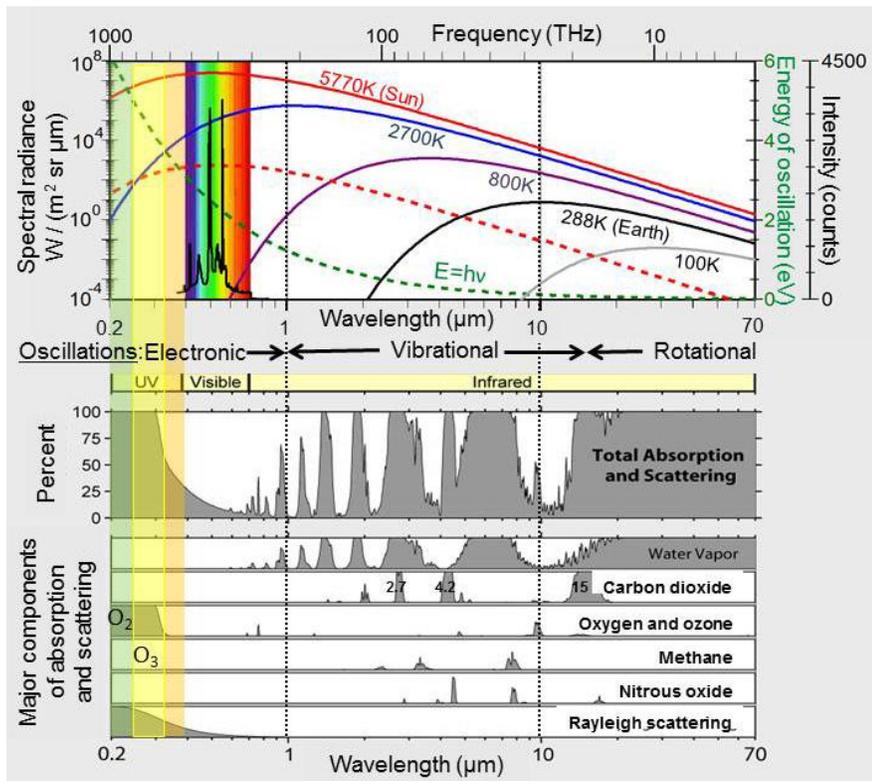
Figure S1 | **The spectral radiance from a black body such as an incandescent light bulb (blue line, 2700K) is over a broad spectrum, while the radiance from a fluorescent light bulb (black line on top of the rainbow of visible light) is confined to very narrow parts of the visible spectrum.** The incandescent light bulb has perceptible heat, the fluorescent bulb does not. Absorption by greenhouse gases shown in the lower part is also confined to very narrow spectral bands[73].

   The blue curve shows the spectrum radiated by a typical incandescent light bulb where the temperature of the tungsten filament is 2700K thermally isolated from the bulb by a partial vacuum. Note how little of the energy radiated is in the visible spectrum (rainbow colors from violet to red, 0.380-0.750 μm). Most energy is in the infrared and this is what we perceive as temperature (heat). The radiation from a typical fluorescent lamp with rare-earth phosphor is shown by the black line overlying the visible spectrum[74]. The y-scale for intensity is not scaled to the spectral radiance. Ultraviolet light generated inside the lamp tube causes the terbium, mercury, and europium coating on the glass tube to fluoresce especially strongly at 0.5424, 0.5465 and 0.6116 μm respectively emitting almost all the radiation within the visible spectral band accompanied by very little heat. This is why fluorescent bulbs produce much more visible light using much less energy than incandescent bulbs and why they do not get as hot. The three spectral peaks have color temperatures of 5341K, 5301K, and 4737K respectively but this is really not temperature as we perceive it. We can think of it as microscopic color temperature representing the frequency of the microscopic oscillation of the terbium, mercury, and europium molecules, but there is no warmth without the broad spectrum of infrared radiation.

   Greenhouse gases similarly absorb narrow spectral ranges of radiation from Earth and Sun shown in the lower half of Fig. S1. The details of the 15 μm peak for carbon dioxide are shown in Fig. S2. Each spectral line has a finite width normally assumed to be a Lorentz line shape. The oscillatory energy in the radiation field is absorbed by increasing the oscillatory energy of each of the normal modes of oscillation for each of the degrees of freedom and various combinations of

15

different degrees of freedom of each absorbing molecule. This oscillatory energy in gas molecules is not perceptible as heat (temperature) until it is converted into translational kinetic energy averaged among all the other gas molecules by the billions of collisions per second that occur in gases near Earth's surface. The efficiency of this conversion is not clear, but by the classical law of equipartition, only some oscillatory energy would be converted. The total amount of energy involved is small compared to the broadband radiation spectrum from Earth.
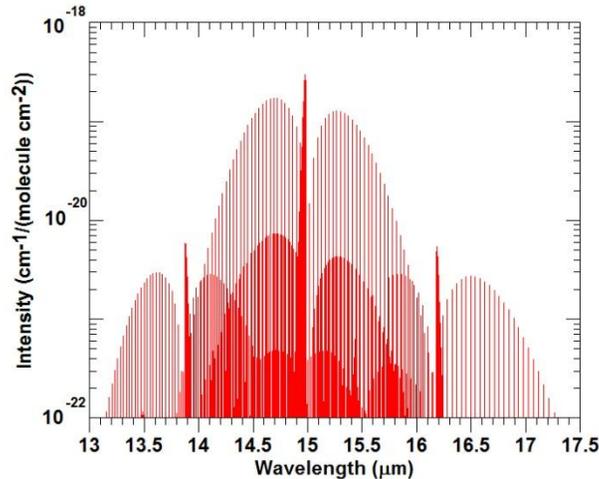
Figure S2 | Absorption of infrared electromagnetic radiation by CO_2 is very selective along spectral lines.

The very narrow spectral lines of absorption imply high-Q resonance such that the oscillatory electromagnetic energy transferred from the field to the molecule at each resonant frequency is equal to one-half the difference between the intensity (spectral radiance) in the field at the resonant frequency and the intensity in the molecule at the same frequency. This means that oscillatory energy (microscopic heat) only flows from higher intensity to lower intensity so as to equalize intensities. When substantial mass "bakes" in sunlight, such as a rock in the desert, the shorter wavelength, higher microscopic color temperature energy must be absorbed by the rock but then heat flows within the rock to raise the temperature of the rock over a wide spectrum such as plotted in the top part of Fig. S1. Thus it does not seem appropriate to assume, as most radiation codes do, that radiation from layers in the atmosphere that are cooler than Earth's surface is absorbed at Earth's surface.

The green shaded band in Fig. S1 shows wavelengths less than 0.242 μm that dissociate molecular oxygen (O_2). The yellow band shows wavelengths between 0.242 μm and 0.310 μm that dissociate ozone (O_3). The orange band shows wavelengths between 0.310 μm and visible light (0.380 μm) that can dissociate O_3 and NO_2 at lower quantum yield. The dashed green line shows Planck's postulate (E=hν). Note how the energy of solar radiation absorbed by a molecule of ozone at a wavelength of 0.310 μm (4.3 eV) is 52 times greater than the energy at 15.0 μm (0.0827 eV) absorbed by a molecule of CO_2 and that all of the energy absorbed to sever the O_3 molecular bond is converted by photodissociation directly into translational kinetic energy (temperature of a gas) while only a fraction of the energy absorbed by CO_2 is converted to temperature through collisions.

Relative timing of pollution
Mean surface temperatures (red line in Fig. S3) increased during the 1930s, cooled during the 1940s, remained relatively constant until 1975, rose rapidly until 1998, and remained relatively

16

constant since. The temperature increase was 30% greater in the northern hemisphere containing 90% of human population and most of the anthropogenic pollution.

SO_2 emissions (black line), 88% from burning fossil fuels[75], rose rapidly until 1973, when concern over acid rain led to the addition of smokestack-scrubbers and other technologies, primarily to electric generating and certain mineral processing facilities, as well as substitution of North Sea oil for coal in Europe. The result was a 20% decrease in SO_2 emissions by 2002. But rapid growth in Asia of industry and particularly electric power generation caused global SO_2 emissions to begin increasing again in 2002.

Tree ring density and thickness normally increase with temperature, but since the 1940s these measures have diverged in northern forests[76]. SO_2 is well-known to stress and even kill trees[77,78]. When anthropogenic SO_2 levels began to decline in the early 1980s, wide-spread greening in northern regions was observed from satellites[79].

NO_X emissions (olive line), 58% from vehicles and 34% from fossil fuels[75], show a similar trend as SO_2 but with a slower decrease in vehicle pollution.
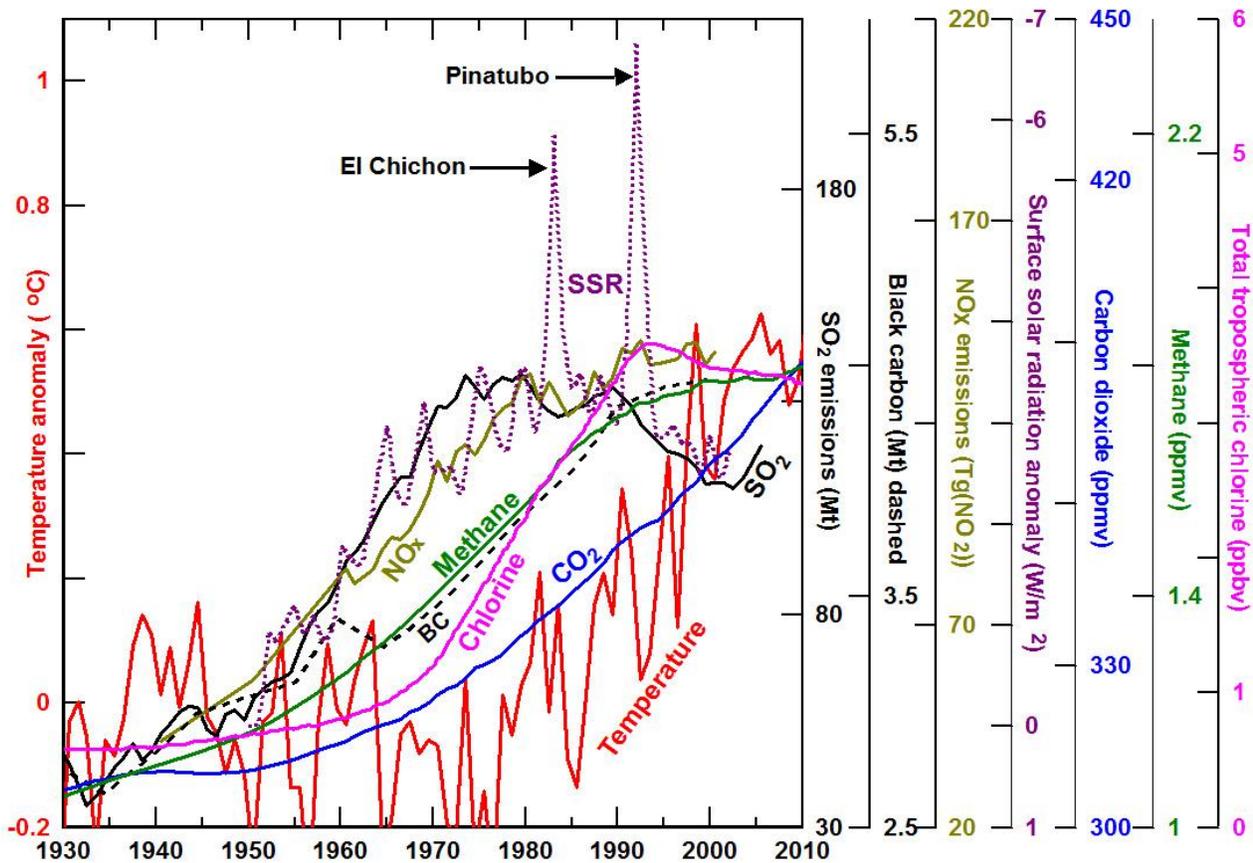
Figure S3 | Increases in temperature and methane concentrations and decreases in surface solar radiation (SSR) reflect increases in pollution (SO_2, NO_X, and black carbon), not the constant rise in CO_2 concentrations. NO_x data from RETRO[80] interpolated before 1960 from US data[81] are thought to be constant or slightly decreasing since 2000[82].

Black carbon emissions (dashed black line)[83], the product of incomplete combustion, began increasing at rates similar to SO_2, dropped precipitously with improvements in diesel-engine design, first applied in this accounting in 1965[84], and leveled off by 2000 as emissions decreased in the West but increased in Asia.

Methane concentrations (green line)[85-87] increased gradually with emissions of other pollutants, reached a relatively constant rate of increase of ~14 ppb/year from 1955 to 1992, stopped increasing by 2006 and began increasing again at a rate of ~6 ppb/year in 2007[85,86]. The lifetime of methane is ~12 years, partially explaining the time lag. Methane concentrations are increased by fossil fuel use[88], biomass burning, certain types of agriculture[89], and thawing of permafrost. Methane is removed from the atmosphere when oxidized by OH. Observed changes in OH concentrations may explain much of the observed changes in methane.

OH concentrations increase with increasing NO_X, tropospheric O_3, and sunlight, and decrease with increasing SO_2, CO, methane, and other pollutants it oxidizes. Global concentrations of OH are difficult to observe and model and are affected by many factors, but modeling suggests they have decreased 9% since preindustrial times[90]. CH_2O data from Greenland suggest OH concentrations may have decreased by as much as 30%[91]. Detailed observations show a gradual decrease from 1980 to 2000[92].

CO in the northern hemisphere increased 0.85%/year from 1950 to 1987[93], decreased very slightly from 1988 (when detailed measurements began) to 2001, and increased slightly to 2005[94].

Concentrations of water vapor and ozone in the lowermost stratosphere increased until 2000 but began decreasing suddenly in 2001[95,96] when emissions of SO_2 stopped declining and began to increase again.

Total tropospheric chlorine caused by anthropogenic chlorofluorocarbons (fuchsia line) increased rapidly after 1970 but reached a peak in 1993 due to implementation of the Montreal Protocol and is expected to return to late-1970s levels by 2040[25].

Annual total column ozone at Arosa, Switzerland (green line, y-axis reversed, Fig. 5), fell rapidly from 1970 to 1994 as a result of the rise in chlorine, and has been increasing until the eruption of Eyjafjallajökull[67].

The purple dotted line (y-axis reversed) shows simulated annual clear-sky surface solar radiation (SSR) anomalies for mid-latitudes in the northern hemisphere[97]. SSR decreased with increasing SO_2 and related pollution and increased with decreasing pollution. SSR decreased rapidly in East Asia after 2000 in phase with dramatic local increases in SO_2 and BC emissions[98]. Note the rapid decreases in SSR for ~3 years following the large volcanic eruptions of El Chichón and Pinatubo.

Yearly CO_2 concentrations rose monotonically (blue line, Fig. 5 and S3)[99,100]. Climate models that assume CO_2 is the primary driver of temperature increase have overestimated global warming since 1998[101,102] and are probably overestimating warming in future decades.

Increases in all these types of pollution did not raise global temperatures until chlorine (fuchsia line) increased, depleting total column ozone (green line, Fig. 5).

Volcanism is a primary driver of climate change

Layers of ice beneath Summit Greenland that contain the largest concentrations of volcanic sulfate per century (red line, Fig. S4)[103] also contain $\delta^{18}O$ evidence[104] for the most rapid global warming (green line) during the Bolling warming (B), decreasing during the cooler Younger Dryas (Y), and increasing again during the Preboreal warming (P). Volcanic sulfate is total sulfate minus the small contributions from sea salt and dust based on sodium and calcium content[105]. Volcanic sulfate forms through oxidation of SO_2 emitted by volcanoes. The rapid increase in "volcanic" sulfate during the 20th century primarily results from anthropogenic emissions of SO_2 (Fig. 5 and S3) from northern Russia, northern Europe, and central North America[106].

This temporal association of SO_2 emissions with warming over the past 25,000 years is unambiguous. Sulfate and the $\delta^{18}O$ proxy for temperature are measured in the same ice layers so there is little error in relative timing. Peak sulfate per century during peak warming (2028 ppb) is

218 times greater than average sulfate per century (9.3 ppb) during the last glacial maximum (LGM, Fig. S4) (21-25 thousand years before present) and 441 times greater than average sulfate (4.6 ppb) between 5 and 1 thousand years before present. 63% of the 7000 ice layers measured contain zero sulfate. Yet nearly all large explosive volcanic eruptions observed throughout written history caused cooling of ~0.5°C for up to 3 years. How can volcanoes be associated with both cooling and warming?
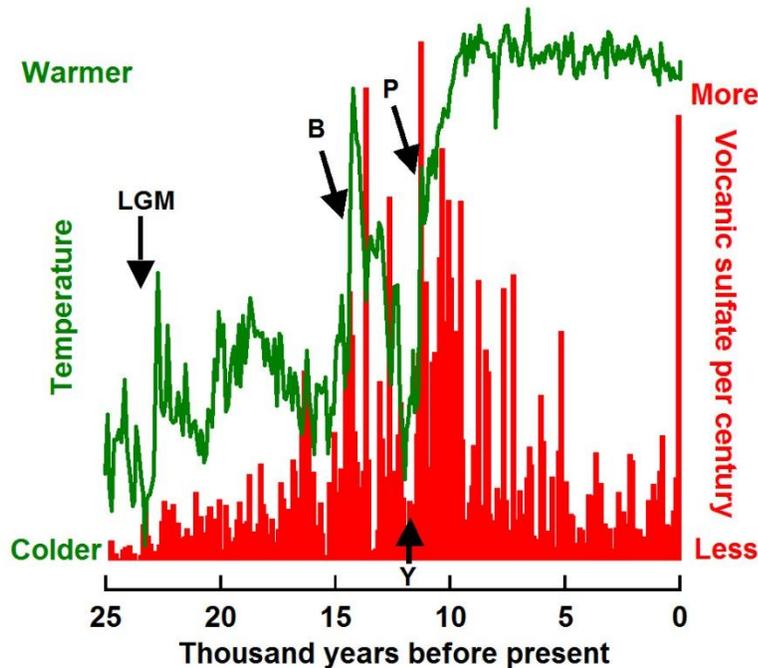
Figure S4 | **Volcanic sulfate per century (red) is unusually high during periods of rapid warming** (green), suggesting volcanism is contemporaneous with global warming. Volcanic sulfate ranges from 0 to 2028 ppb. "Volcanic" sulfate in the 20th century is cause primarily by anthropogenic emissions. The value shown (1910 ppb) is twice the sum observed during the 50 years from 1935 through 1984. The increase in equatorial Pacific sea surface temperature since the last glacial maximum (LGM) is on the order of 2.8°C[107].

This enigma has driven my research since 2006. In 2009, I published a paper[60] documenting the association of volcanism with global warming, global cooling, mass extinctions, and drought and proposed that the differences were due to different rates of volcanism and the chemical effects of SO_2. More recent research described in this paper shows that SO_2 does not cause warming directly (Fig. 5) but that oxidized SO_2 (sulfate) is the footprint of the level of volcanic activity recorded in glacial ice and that the enigma is explained by the balance of ozone depletion versus stratospheric aerosols. Hegerl et al.[108] similarly found that detailed reconstructions of global temperature over the past 1500 years suggest that "natural forcing, particularly by volcanism, explains a substantial fraction of decadal variance." What are the details of these mechanisms?

Volcanoes erupting andesitic, dacitic and other evolved magmas typically eject 5 to 25 Mt SO_2 into the lower stratosphere where it is oxidized by OH to form sulfuric acid with an e-folding time of ~35 days[109] but up to 13 months in the Arctic[110]. Sulfuric acid has a very low vapor pressure, aggregating rapidly on particles. Growth of these particles is enhanced in the non-turbulent stratosphere where solar and chemical warming leads to continued lofting and settling evidenced by the very low thermal gradient in the lowermost stratosphere (Fig. 1).

Several months after the 1991 eruption of Pinatubo, particle sizes were typically 300 to 500 nm, reflecting, Mie scattering, and absorbing sunlight, warming the stratosphere 2-3°C within 4-5 months (purple line, Fig. 3), and cooling Earth up to 0.5°C for three years[111]. These stratospheric aerosols decreased average total solar irradiance at Earth's surface by less than 1%[112]. Modeling shows that such cooling may have affected ocean temperatures for more than 100 years following the VEI=6 eruption of Krakatoa in 1883[113] and that cooling can accumulate over many eruptions[114] incrementing the globe into an ice age when rates of major explosive volcanism are 5 to 10 times more active than throughout written history[60]. SO_2 is widely assumed to have the same cooling effect in the troposphere, but this seems highly unlikely. With an e-folding time of 35 days to be oxidized, SO_2 is spread around the world and replenished continuously by anthropogenic emissions[115,116]. Furthermore the particle sizes cannot grow large enough to reflect significant amounts of sunlight due to turbulence except possibly by circulation in certain types of clouds.

These large volcanic eruptions also deplete total column ozone for up to a decade, but the absorption, reflection and scattering of sunlight by the aerosols is more dominant for the first few years except during northern winters where and when ozone depletion is greatest. Temperatures over large parts of continents in the northern hemisphere, increase by as much as 3°C during the two winters following the 1991 eruption of Pinatubo[31].

Volcanoes on oceanic islands such as Iceland and Hawaii, erupt more primitive basaltic magmas, extrude cubic kilometers of lava flows on the surface, display impressive lava fountains often along kilometers of linear vents, emit megatons of SO_2 and halogens such as chlorine, bromine, and fluorine, but rarely eject these gases into the stratosphere. Global warming predominates because ozone depletion is substantial and cooling by aerosols is minimal.

Warming was clearly observed during the ten eruptive phases of the basaltic fissure volcano Laki (Lakagigar) in South Iceland from June 8, 1783 until February 7, 1784[117], the largest basaltic lava flow in written history except for the eruption of nearby Eldgjá in 934 A.D. Laki ejected ~24 Mt of SO_2 into the lower stratosphere where it most likely spread eastward and northward ultimately providing cooling. Pinatubo only erupted ~17 Mt SO_2, but Laki ejected an additional ~96 Mt SO_2 into the troposphere where the jet stream carried much of it southeastward to Europe. Severe acid damage to vegetation from Iceland to Eastern Europe, to Italy suggests concentrations of SO_2 could have been as high as 1,000 ppb[117], roughly three orders of magnitude larger than background. A "dry fog" blanketed much of Europe primarily from June 14 through August. "Many people experienced troublesome headaches, respiratory difficulties, and asthma attacks"[117]. SO_2 is invisible but when absorbing ultraviolet radiation, the electronic transitions cause fluorescence in the visible spectrum explaining this "dry fog". In July, surface temperatures increased as much as 3.3°C above the 30-year mean centered on 1783, the highest temperatures recorded from the first measurements in 1659 until 1983[117,118]. There was not time for significant amounts of aerosol to form in the stratosphere nor for ozone to be depleted by chlorine released through heterogeneous processes. But the eruption did release ~7 Mt of hydrochloric acid and ~15 Mt of hydrofluoric acid[119] that could have caused rapid depletion of ozone.

The Laki eruption deposited ~115 ppb sulfate in snow at Summit Greenland[103]. During the major Preboreal warming (P in Fig. S4) (11,700-9,800 years before present), sulfate per century in this ice was as much as 2028 ppb, 18 times more than from Laki. Laki-type activity continuing for these 1900 years appears to have played a major role in finally warming the oceans out of the last ice age. Basaltic volcanism under ice leads to long, flat-topped, steep-sided table mountains or tuyas found throughout Iceland. "12 of the 13 dated table mountains experienced their final eruptive phase during the last deglaciation"[120].

Volcanism was similarly highest during the other 13 Dansgaard-Oeschger sudden warmings between 46,000 and 11,600 years before present when tropical sea-surface temperatures rose ~3°C

in a decade or two and then decreased back to ice-age temperatures over decades to centuries as volcanism waned before the deep ocean could be warmed[60,121,122].

The Late Paleocene thermal maximum (54.18-53.90 Ma, million years before present) is contemporaneous with the massive sub-aerial volcanism during the opening of the North Atlantic Ocean[123].

Laki extruded 12.3 km^3 of lava flowing over an area of 565 km^2. Every 25 million years, on average, there have been massive eruptions of millions of cubic kilometers of basalt typically associated with major mass extinctions[60,124,125]. The Siberian Traps, for example, extruded ~250 Ma, cover an area today larger than the states of Washington, Oregon, California, Idaho, Nevada, and Arizona combined and when forming may have covered an area as large as 71% of the size of the United States[126]. Visscher et al.[127] document increased mutations in herbaceous lycopsids during the end-Permian mass extinction that imply substantial depletion of ozone.

The location, volume, type, and timing of volcanism are determined by the motion of large lithospheric plates (plate tectonics). Sub-aerial basaltic eruptions are most common on islands along mid-ocean ridges and places where these ridges are overrun by continents. Major explosive volcanoes are most common where oceanic plates are being subducted beneath continents, such as around most of the Pacific Ocean. Explosive eruptions generally cool Earth, incrementing it into an ice age if sufficiently frequent; basaltic eruptions generally warm Earth[60]. Basaltic eruptions deep under oceans do not appear to influence climate directly, but major increases in the area of ocean crust formed per year at 33.9, 12, and 3 Ma, imply major increases in rates of subduction are associated with major cooling[60,128]. Sulfate and ash in ice cores record the level of volcanism faithfully, but the ratio of stratospheric aerosols to ozone depletion controls the effects of this volcanism on temperature.

Apparent increase in ozone before large volcanic eruptions

Annual total column ozone observed at Arosa appears to have increased 12 DU (3.9%) in 1991 when Pinatubo erupted but decreased 28 DU (8.5%) by 1993 (Fig. 3). Similarly ozone appears to have increased 14 DU (4.4%) in 2010 when Eyjafjallajökull erupted but decreased 28 DU (8.4%) in 2011. Other volcanic eruptions shown in Fig. 3 are also contemporaneous with a modest increase in ozone followed the next year by a much larger decrease.

The ozone increase in 2010 occurred primarily between February 19 and February 26, ~4 weeks before the first effusive flank eruption of basalt from March 20 to April 12 and ~7 weeks before the main explosive eruption of trachyandesite on April 14. Fig. S5 shows that total ozone northeast of Iceland increased to more than 550 DU on February 19 over a background of ~325 DU, an increase of ~70%[8]. The deviation of total ozone over the period from February 21 to February 28 increased 45% compared to mean levels from 1978 thru 1988 (Fig. S6)[8].

At Eyjafjallajökull, seismic activity and deformation began in December, 2009, "explained by a single horizontal sill inflating at a depth of 4.0-5.9 km under the southeastern flank of the volcano"[129]. Deformation increased exponentially in February, suggesting a major change in pressure conditions within the system by March 4. Thus a substantial release of gas from the top of the magma body is highly likely to have occurred in late February as the roof of the intrusion fractured to the surface.

Ozone is not a likely volcanic gas because magma has a reduced oxidation state at high temperature. Primary gases observed from high-temperature fumaroles include SO_2, which absorbs ultraviolet solar radiation strongly at the same wavelengths as ozone (Fig. 2) and is known to affect ozone measurements in urban areas such as Uccle, just outside of Brussels, Belgium[130]. Basaltic effusive eruptions typically emit 10 to 100 times more SO_2 per cubic kilometer of magma than the more explosive eruptions from volcanoes such as Pinatubo with more evolved magmas[42,131,132]. SO_2

is colorless so that its release from high-temperature fumaroles in the vicinity of the effusive eruption that began on March 20 would have gone unnoticed if substantial water vapor was not included. There were no instruments in the vicinity to detect it.
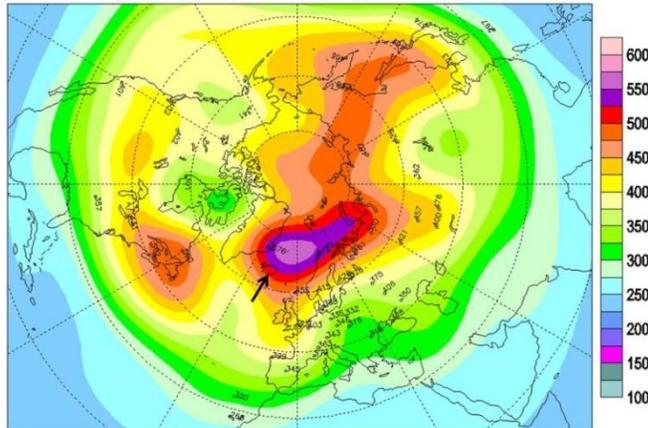
Figure S5 | A total ozone anomaly >550 DU was observed northeast of Iceland (black arrow) on February 19, 2010, based on the satellite borne Total Ozone Mapping Spectrometer (TOMS) integrated with data from ground stations.
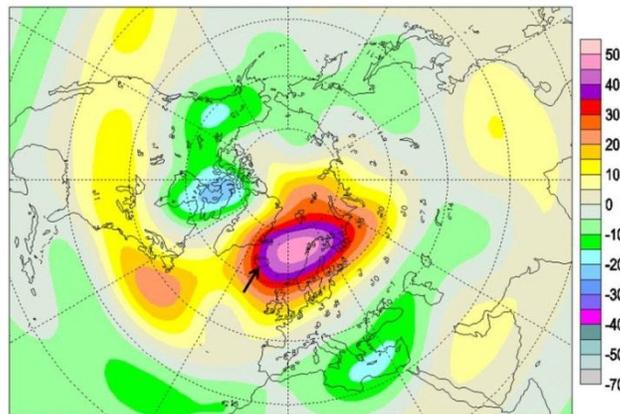
Figure S6 | The deviation of total ozone observed northeast of Iceland (black arrow) from February 20 through 28, 1991, from the mean of 1978-1988 levels was as high as 50%.

Another possibility is that high-temperature gases from basaltic magma (1300-1400°C)[133] may interact in some way with water released from the magma, with ground water, or even with atmospheric water vapor to form oxygen atoms and thus ozone. Magmatic high-temperature gases might also interact with volatile organic compounds or nitrogen compounds or gases to form ozone catalytically.

Local farmers noted unusual melting of snow near high temperature fumaroles "months" before the eruption of Hekla in south Iceland on May 5, 1970[134,135].

Mt. Pinatubo in the Philippines (120°E) showed signs of reawakening with a group of felt earthquakes on March 15, 1991, the first steam explosions on April 2, first eruption on June 12, and the main eruption on June 15. Ozone anomalies >525 DU occurred from late January, 1991, through April 25, primarily at latitudes >50°N. The Brewer-Dobson circulation is thought to move ozone and related gases from the latitude of Pinatubo (15°N) up into the stratosphere, northward, and then

22

downward north of 50°N[136136]. The spatial and temporal correlations are not as clear as for Eyjafjallajökull because while Pinatubo was a much larger explosive eruption, the changes in the magmatic plumbing system are not as well-known and the magma was not basaltic.

Maps of total ozone such as in Fig. S5 are produced daily and could prove useful in determining when intruding magmas begin to release gases to the surface, especially for basaltic magmas, but extensive work is still needed to map the nature of these large apparent ozone anomalies and to understand their chemistry.

Modeling

Observations in this paper include:
1. photodissociation of O_2 and O_3 warms the stratosphere,
2. depletion of total column ozone moves this warming down into the troposphere cooling the lower stratosphere,
3. the lower stratosphere cooled more than 2°C since 1957,
4. mean surface temperatures in the Northern Hemisphere increased ~0.8°C during the same time period as stratospheric cooling,
5. stratospheric cooling occurred primarily in steps following the times of major volcanic eruptions, and
6. greatest regional increases in surface temperatures occurred at the times and locations of the greatest depletion of ozone.

Modeling these observed changes accurately will require understanding at least:
1. seasonal and yearly timing and location of ozone depletion caused by all volcanic eruptions, ongoing volcanic emissions, and anthropogenic chlorofluorocarbons,
2. effects of ozone depletion on transmission of ultraviolet energy through the atmosphere,
3. efficiency of converting that radiation to temperature in a polluted atmosphere, in the ocean, and on land with varying albedo,
4. efficiency of radiation from land, water, ice, and snow at night,
5. effects of solar zenith angle not only on energy per square meter, but also on increasing the path length over which photodissociation can occur,
6. partitioning of energy absorbed in a polluted environment to warm the air versus energy absorbed directly by land and by ocean to warm the climate system,
7. efficiency of transmission of ultraviolet radiation through clouds, water vapor, and water, and
8. feedbacks such as the effects of a cooling stratosphere caused by ozone depletion on increasing that depletion,
9. whether absorption of radiation not energetic enough to cause photodissociation can have any significant effect on atmospheric temperatures and
10. whether heat can be moved by radiation to warmer bodies as assumed in current radiation codes.

References
1 Fioletov, V. Ozone climatology, trends, and substances that control ozone. *Atmos. Ocean* **46**, 39-67 (2008).
2 Folland, C. K. *et al.* in *Climate Change 2001: The Scientific Basis. Contribution of Working Group I to the Third Assessment Report of the Intergovernmental Panel on Climate Change* (eds J.T. Houghton *et al.*) 99-181 (Cambridge University Press, 2001).
3 Trenberth, K. E. *et al.* in *Climate Change 2007: The Physical Science Basis. Contribution of Working Group I to the Fourth Assessment Report of the Intergovernmental Panel on Climate Change* (eds S. Solomon *et al.*) 235-336 (Cambridge University Press, 2007).
4 Kinnison, D. *et al.* Sensitivity of chemical tracers to meteorological parameters in the MOZART-3 chemical transport model. *J. Geophys. Res* **112**, D20302 (2007).
5 Seidel, D. J. & Randel, W. J. Variability and trends in the global tropopause estimated from radiosonde data. *J. Geophys. Res.* **111**, D21101 (2006).
6 *HadCRUT3_NH*, <www.cru.uea.ac.uk/cru/data/temperature/hadcrut3nh.txt> (2012).
7 Reed, R. J. The role of vertical motion in ozone-weather relationship. *J. Meteorol.* **7**, 263-267 (1950).
8 Environment Canada. *Archive of world ozone maps*, <exp-studies.tor.ec.gc.ca/clf2/e/ozoneworld.html> (2012).
9 Madronich, S. in *The Role of the Stratosphere in Global Change* Vol. 8, NATO ASI Series I: Global Environmental Change (ed M.L. Chanin) 463-471 (Springer-Verlag, 1993).
10 Trenberth, K. E., Fasullo, J. T. & Kiehl, J. Earth's Global Energy Budget. *Bull. Am. Meteorol. Soc.* **90**, 311-323 (2009).
11 Matsumi, Y. *et al.* Quantum yields for production of $O(^1D)$ in the ultraviolet photolysis of ozone: Recommendation based on evaluation of laboratory data. *J. Geophys. Res.* **104**, 12 (2002).
12 Sander, S. P. *et al.* *Chemical Kinetics and Photochemical Data for Use in Atmospheric Studies Evaluation Number 15*. Vol. 06-2 (Jet Propulsion Laboratory, 2006).
13 Tedetti, M. & Sempéré, R. Penetration of ultraviolet radiation in the marine environment. A review. *Photochemistry and Photobiology* **82**, 389-397 (2006).
14 Hughes, G. L., Rao, S. S. & Rao, T. S. Statistical analysis and time-series models for minimum/maximum temperatures in the Antarctic Peninsula. *Proc. Roy. Soc. London, Ser. A* **463**, 241-259 (2007).
15 Mulvaney, R. *et al.* Recent Antarctic Peninsula warming relative to Holocene climate and ice-shelf history. *Nature* **489**, 141-144 (2012).
16 Meredith, M. P. & King, J. C. Rapid climate change in the ocean west of the Antarctic Peninsula during the second half of the 20th century. *Geophys. Res. Lett* **32**, L19604 (2005).
17 Clarke, A. *et al.* Climate change and the marine ecosystem of the western Antarctic Peninsula. *Phil. Trans. R. Soc. London, Ser. B* **362**, 149-166 (2007).
18 Stammerjohn, S. E., Martinson, D. G., Smith, R. C. & Iannuzzi, R. A. Sea ice in the western Antarctic Peninsula region: Spatio-temporal variability from ecological and climate change perspectives. *Deep Sea Res. II* **55**, 2041-2058 (2008).
19 Wang, X. & Zender, C. S. Arctic and Antarctic diurnal and seasonal variations of snow albedo from multiyear Baseline Surface Radiation Network measurements. *J. Geophys. Res.* **116**, F03008 (2011).
20 Manney, G. L. *et al.* Unprecedented Arctic ozone loss in 2011. *Nature* **478**, 469 (2011).
21 Kwok, R. & Untersteiner, N. The thinning of Arctic sea ice. *Physics Today* **64**, 36-41 (2011).

24

22   NSIDC. *Arctic sea ice reaches lowest extent for the year and the satellite record*, <nsidc.org/news/press/2012_seaiceminimum.html> (2012).

23   Lemke, P. *et al.* in *Climate Change 2007: The physical science basis* (eds S. Solomon *et al.*) 337-383 (Cambridge University Press, 2007).

24   A. Douglass et al., in Scientific Assessment of Ozone Depletion: 2010. (World Meteorological Organization Global Ozone Research and Monitoring Project - Report No. 52, 2011) Figure 2-2.

25   Solomon, S. Stratospheric ozone depletion: A review of concepts and history. *Rev. Geophys.* **37**, 275-316 (1999).

26   *Multivariate ENSO index (MEI)*, <www.esrl.noaa.gov/psd/enso/mei/> (2012).

27   Druitt, T. Emplacement of the 18 May 1980 lateral blast deposit ENE of Mount St. Helens, Washington. *Bull. Volcanol.* **54**, 554-572 (1992).

28   Gleason, J. *et al.* Record low global ozone in 1992. *Science* **260**, 523 (1993).

29   Angell, J. K. Estimated impact of Agung, El Chichon and Pinatubo volcanic eruptions on global and regional total ozone after adjustment for the QBO. *Geophys. Res. Lett.* **24**, 647–650 (1997).

30   Kerr, J., Wardle, D. & Tarasick, D. Record low ozone values over Canada in early 1993. *Geophys. Res. Lett.* **20**, 1979-1982 (1993).

31   Robock, A. Pinatubo eruption: The climatic aftermath. *Science* **295**, 1242-1244 (2002).

32   De Mazière, M. *et al.* Quantitative evaluation of the post–Mount Pinatubo NO_2 reduction and recovery, based on 10 years of Fourier transform infrared and UV-visible spectroscopic measurements at Jungfraujoch. *J. Geophys. Res.* **103**, 10849-10810,10858 (1998).

33   Johnston, P., McKenzie, R., Keys, J. & Matthews, W. Observations of depleted stratospheric NO_2 following the Pinatubo volcanic eruption. *Geophys. Res. Lett.* **19**, 211-213 (1992).

34   Coffey, M. T. Observations of the impact of volcanic activity on stratospheric chemistry. *J. Geophys. Res.* **101**, 6767–6780 (1996).

35   Thompson, D. W. J. & Solomon, S. Understanding recent stratospheric climate change. *J. Clim.* **22**, 1934-1943 (2009).

36   Randel, W. J. in *The Stratosphere: Dynamics, Transport and Chemistry, Geophysical Monograph Series* Vol. 190 (eds L. M. Polvani, A. H. Sobel, & D. W. Waugh) 123-135 (AGU, 2010).

37   Angell, J. K. Stratospheric warming due to Agung, El Chichón, and Pinatubo taking into account the quasi-biennial oscillation. *J. Geophys. Res.* **102**, 9479–9486 (1997).

38   Anderson, J. G., Wilmouth, D. M., Smith, J. B. & Sayres, D. S. UV Dosage Levels in Summer: Increased Risk of Ozone Loss from Convectively Injected Water Vapor. *Science* **337**, 835-839 (2012).

39   SPARC. *The Role of Halogen Chemistry in Polar Stratospheric Ozone Depletion*, <www.atmosp.physics.utoronto.ca/SPARC/HalogenChem_Final_20090213.pdf> (2009).

40   Molina, M. J. & Rowland, F. S. Stratospheric sink for chlorofluoromethanes: Chlorine catalysed destruction of ozone. *Nature* **249**, 810-814 (1974).

41   Tabazadeh, A. & Turco, R. P. Stratospheric chlorine injection by volcanic eruptions: HCl scavenging and implications for ozone. *Science* **260**, 1082-1084 (1993).

42   Self, S., Blake, S., Sharma, K., Widdowson, M. & Sephton, S. Sulfur and chlorine in late Cretaceous Deccan magmas and eruptive gas release. *Science* **319**, 1654-1657 (2008).

43   Vance, A. *et al.* Ozone depletion in tropospheric volcanic plumes. *Geophys. Res. Lett.* **37** (2010).

44   von Glasow, R. Atmospheric chemistry in volcanic plumes. *Proc. Nat. Acad. Sci. U.S.A.* **107**, 6594-6599 (2010).

45   NOAA. *U.S. Records*, <www.ncdc.noaa.gov/extremes/records/daily/maxt/2012/03/00?sts[]=US> (2012).

46   Minnis, P. *et al.* Radiative climate forcing by the Mount Pinatubo eruption. *Science* **259**, 1411-1415 (1993).

47   *Sea Surface Temperatures Reach Record Highs on Northeast Continental Shelf*, <www.nefsc.noaa.gov/press_release/2012/SciSpot/SS1209/> (2012).

48   Global Volcanism Program. *Large Holocene eruptions*, <www.volcano.si.edu/world/largeeruptions.cfm> (2012).

49   NASA. *Sunspot number per month*, <solarscience.msfc.nasa.gov/greenwch/spot_num.txt> (2012).

50   Haigh, J. D., Winning, A. R., Toumi, R. & Harder, J. W. An influence of solar spectral variations on radiative forcing of climate. *Nature* **467**, 696-699 (2010).

51   Trenberth, K. E. An imperative for climate change planning: tracking Earth's global energy. *Curr. Opin. Environ. Sustain.* **1**, 19-27 (2009).

52   Knight, J. *et al.* in *State of the Climate in 2008* Vol. 90 (eds T. C. Peterson & M. O. Baringer) S22-S23 (Bull. Am. Meteorol. Soc., 2009).

53   Hansen, J. *et al.* Climate response times: dependence on climate sensitivity and ocean mixing. *Science* **229**, 857 (1985).

54   Domingues, C. M. *et al.* Improved estimates of upper-ocean warming and multi-decadal sea-level rise. *Nature* **453**, 1090-1093 (2008).

55   LaRiviere, J. P. *et al.* Late Miocene decoupling of oceanic warmth and atmospheric carbon dioxide forcing. *Nature* **486**, 97-100 (2012).

56   Berner, R. A. Phanerozoic atmospheric oxygen: New results using the GEOCARBSULF model. *Am. J. Sci.* **309**, 603 (2009).

57   Seidel, D. J., Fu, Q., Randel, W. J. & Reichler, T. J. Widening of the tropical belt in a changing climate. *Nat. Geosci.* **1**, 21-24 (2008).

58   Polvani, L. M., Waugh, D. W., Correa, G. J. P. & Son, S. W. Stratospheric ozone depletion: The main driver of twentieth-century atmospheric circulation changes in the Southern Hemisphere. *J. Clim.* **24**, 795-812 (2011).

59   Allen, R. J., Sherwood, S. C., Norris, J. R. & Zender, C. S. Recent Northern Hemisphere tropical expansion primarily driven by black carbon and tropospheric ozone. *Nature* **485**, 350-354 (2012).

60   Ward, P. L. Sulfur dioxide initiates global climate change in four ways. *Thin Solid Films* **517**, 3188-3203 (2009).

61   Committee on Extension to the Standard Atmosphere. *U.S. Standard Atmosphere, 1976*. (U.S. Government Printing Office, 1976).

62   Krueger, A. J. & Minzner, R. A. A mid-latitude ozone model for the 1976 US standard atmosphere. *J. Geophys. Res.* **81**, 4477-4481 (1976).

63   Rothman, L. S. *et al.* The HITRAN 2008 molecular spectroscopic database. *J. Quant. Spectrosc. Radiat. Transfer* **110**, 533-572 (2009).

64   Hermans, C., Vandaele, A. C. & Fally, S. Fourier transform measurements of SO_2 absorption cross sections:I. Temperature dependence in the 24000–29000cm−1 (345–420nm) region. *J. Quant. Spectrosc. Radiat. Transfer* **110**, 756-765 (2009).

65   Vandaele, A. C., Hermans, C. & Fally, S. Fourier transform measurements of SO_2 absorption cross sections: II.Temperature dependence in the 29000–44000cm−1 (227–345nm) region. *J. Quant. Spectrosc. Radiat. Transfer* **110**, 2115-2126 (2009).

66   Finlayson-Pitts, B. J. & Pitts, J. N. *Chemistry of the Upper and Lower Atmosphere: Theory, Experiments, and Applications*. (Academic Press, 1999).

67   Staehelin, J. *et al.* Total ozone series at Arosa (Switzerland): Homogenization and data comparison. *J. Geophys. Res.* **103**, 5827-5841 (1998).

68   Levitus, S. *et al.* World ocean heat content and thermosteric sea level change (0-2000 m), 1955-2010. *Geophys. Res. Lett.* **39**, in press (2012).

69   Hadley Centre. *HadAT: globally gridded radiosonde temperature anomalies from 1958 to present*, <www.metoffice.gov.uk/hadobs/hadat/images.html> (2012).

70   Remote Sensing Systems. <www.remss.com/msu/msu_data_description.html> (2012).

71   Douglass, A. *et al.* in *Scientific Assessment of Ozone Depletion: 2010* (ed C. A. Ennis) 76 (World Meteorological Organization Global Ozone Research and Monitoring Project - Report No. 52, 2011).

72   Smith, S. J. *et al.* Anthropogenic sulfur dioxide emissions: 1850–2005. *Atmos. Chem. Phys.* **11**, 1101-1116 (2011).

73   Rohde, R. A. *Radiation transmitted by the atmosphere*, <commons.wikimedia.org/wiki/File:Atmospheric_Transmission.png> (2012).

74   *Fluorescent lamp: Phosphors and the spectrum of emitted light*, <en.wikipedia.org/wiki/Fluorescent_lamp#Phosphors_and_the_spectrum_of_emitted_light> (2012).

75   EPA. *Air emission sources*, <www.epa.gov/air/emissions/> (2012).

76   D'Arrigo, R., Wilson, R., Liepert, B. & Cherubini, P. On the 'Divergence Problem'in Northern Forests: A review of the tree-ring evidence and possible causes. *Global Planet. Change* **60**, 289-305 (2008).

77   Keller, T. Direct effects of sulphur dioxide on trees. *Phil. Trans. R. Soc. London, Ser. B* **305**, 317-325 (1984).

78   Manninen, S. & Huttunen, S. Response of needle sulphur and nitrogen concentrations of Scots pine versus Norway spruce to SO_2 and NO_2. *Environ. Pollut.* **107**, 421-436 (2000).

79   Nemani, R. *et al.* Climate-driven increases in global terrestrial net primary production from 1982 to 1999. *Science* **300**, 1560 (2003).

80   Schultz, M. & Rast, S. *REanalysis of the TROpospheric chemical composition over the past 40 years,*, <retro.enes.org/reports/D1-6_final.pdf > (2008).

81   U. S. Environmental Protection Agency. *National Air Pollutant Emission Trends, 1900 - 1998.* (2000).

82   Cofala, J., Rafaj, P., Schöpp, W., Klimont, Z. & Amann, M. *Emissions of Air Pollutants for the World Energy Outlook 2009 Energy Scenarios*, <worldenergyoutlook.org/docs/Emissions_of_Air_Pollutants_for_WEO2009.pdf> (2009).

83   Bond, T. C. *et al.* Historical emissions of black and organic carbon aerosol from energy-related combustion, 1850–2000. *Global Biogeochem. Cycles* **21**, GB2018 (2007).

84   Novakov, T. *et al.* Large historical changes of fossil-fuel black carbon aerosols. *Geophys. Res. Lett.* **30**, 1324 (2003).

85   Dlugokencky, E. J. *Carbon dioxide, nitrous oxide, methane, CFC-12, CFC-11*, <www.esrl.noaa.gov/gmd/aggi/aggi_2010.fig2.png> (2010).

86   Etheridge, D. M., Steele, L. P., Francey, R. J. & Langenfelds, R. L. Atmospheric methane between 1000 A.D. and present: Evidence of anthropogenic emissions and climatic variability *J. Geophys. Res.* **103**, 15979-15993 (1998).

87   Dlugokencky, E. J. *et al.* Observational constraints on recent increases in the atmospheric CH_4 burden. *Geophys. Res. Lett.* **36**, L18803 (2009).

88   Aydin, M. *et al.* Recent decreases in fossil-fuel emissions of ethane and methane derived from firn air. *Nature* **476**, 198-201 (2011).

89   Kai, F. M., Tyler, S. C., Randerson, J. T. & Blake, D. R. Reduced methane growth rate explained by decreased Northern Hemisphere microbial sources. *Nature* **476**, 194-197 (2011).

90   Wang, Y. & Jacob, D. J. Anthropogenic forcing on tropospheric ozone and OH since preindustrial times. *J. Geophys. Res.* **D23**, 31123-31136 (1998).

91   Staffelbach, T., Neftel, A., Stauffer, B. & Jacob, D. Formaldehyde in polar ice cores: a possibility to characterize the atmospheric sink of methane in the past. *Nature* **349**, 603-605 (1991).

92   Bousquet, P., Hauglustaine, D. A., Peylin, P., Carouge, C. & Ciais, P. Two decades of OH variability as inferred by an inversion of atmospheric transport and chemistry of methyl chloroform. *Atmos. Chem. Phys.* **5**, 1679-1731 (2005).

93   Zander, R., Demoulin, P., Ehhalt, D., Schmidt, U. & Rinsland, C. Secular increase of the total vertical column abundance of carbon monoxide above central Europe since 1950. *J. Geophys. Res.* **94**, 11021-11011,11028 (1989).

94   Duncan, B. N. *et al.* Global budget of CO, 1988–1997: Source estimates and validation with a global model. *J. Geophys. Res.* **112**, D22301 (2007).

95   Randel, W. J., Wu, F., Vömel, H., Nedoluha, G. E. & Forster, P. Decreases in stratospheric water vapor after 2001: Links to changes in the tropical tropopause and the Brewer-Dobson circulation. *J. Geophys. Res.* **111**, D12312 (2006).

96   Solomon, S. *et al.* Contributions of stratospheric water vapor to decadal changes in the rate of global warming. *Science* **327**, 1219-1223 (2010).

97   Wild, M. Global dimming and brightening: A review. *J. Geophys. Res.* **114**, D00D16 (2009).

98   Lu, Z. *et al.* Sulfur dioxide emissions in China and sulfur trends in East Asia since 2000. *Atmos. Chem. Phys.* **10**, 8657-8715 (2010).

99   Etheridge, D. M. *et al. Historical CO₂ record from the Law Dome DE08, DE08-2, and DSS ice cores*, <cdiac.ornl.gov/ftp/trends/co2/lawdome.combined.dat> (1998).

100   NOAA ESRL. *Trends in atmospheric carbon dioxide*, <www.esrl.noaa.gov/gmd/ccgg/trends/#mlo_full> (2010).

101   Trenberth, K. & Fasullo, J. Tracking Earth's Energy. *Science* **328**, 316 (2010).

102   Hansen, J. *et al.* Earth's energy imbalance: Confirmation and implications. *Science* **308**, 1431-1435 (2005).

103   Zielinski, G. A., Mayewski, P. A., Meeker, L. D., Whitlow, S. & Twickler, M. A 110,000-year record of explosive volcanism from the GISP2 (Greenland) ice core. *Quat. Res.* **45**, 109 (1996) (ftp.ncdc.noaa.gov/pub/data/paleo/icecore/greenland/summit/gisp2/chem/volcano.txt1996).

104   White, J. W. C. *et al.* The climate signal in the stable isotopes of snow from Summit, Greenland: Results of comparisons with modern climate observations. *J. Geophys. Res.* **102**, 26425 (1997) (ftp.ncdc.noaa.gov/pub/data/paleo/icecore/greenland/summit/gisp2/isotopes/stacked.txt).

105   Mayewski, P. A. *et al.* Major features and forcing of high-latitude northern hemisphere atmospheric circulation using a 110,000-year-long glaciochemical series. *J. Geophys. Res.* **102**, 26345–26366 (1997).

106   Barrie, L., Hoff, R. & Daggupaty, S. The influence of mid-latitudinal pollution sources on haze in the Canadian Arctic. *Atmos. Environ.* **15**, 1407-1419 (1981).

107   Lea, D. W. Climate Impact of Late Quaternary Equatorial Pacific Sea Surface Temperature Variations. *Science* **289**, 1719-1724 (2000).

108   Hegerl, G. C. *et al.* Detection of human influence on a new, validated 1500-year temperature reconstruction. *J. Clim.* **20**, 650-666 (2007).

109   Bluth, G. J. S., Doiron, S. D., Schnetzler, C. C., Krueger, A. J. & Walter, L. S. Global tracking of the SO_2 clouds from the June, 1991 Mount Pinatubo eruptions. *Geophys. Res. Lett.* **19**, 151-154 (1992).

110   Stone, R. S., Keys, J. & Dutton, E. G. Properties and decay of stratospheric aerosols in the Arctic following the 1991 eruptions of Mount Pinatubo. *Geophys. Res. Lett.* **20**, 2539-2362 (1993).

111   Self, S., Zhao, J.-X., Holasek, R. E., Torres, R. C. & King, A. J. in *Fire and Mud: Eruptions and lahars of Mount Pinatubo, Philippines* (eds Christopher G. Newhall & Raymundo S. Punongbayan) 1089-1115 (Philippine Institute of Volcanology and Seismology and University of Washington Press, 1996).

112   Stenchikov, G. *et al.* Arctic Oscillation response to volcanic eruptions in the IPCC AR4 climate models. *J. Geophys. Res.* **111**, D07107 (2006).

113   Gleckler, P. J. *et al.* Krakatoa's signature persists in the ocean. *Nature* **439**, 675 (2006).

114   Gregory, J. M., Lowe, J. A. & Tett, S. F. B. Simulated global-mean sea level changes over the last half-millennium. *J. Clim.* **19**, 4576-4591 (2006).

115   Fiedler, V. *et al.* East Asian SO_2 pollution plume over Europe–Part 1: Airborne trace gas measurements and source identification by particle dispersion model simulations. *Atmos. Chem. Phys.* **9**, 4717–4728 (2009).

116   Fiedler, V. *et al.* East Asian SO_2 pollution plume over Europe-Part 2: Evolution and potential impact. *Atmos. Chem. Phys.* **9**, 4729-4745 (2009).

117   Thordarson, T. & Self, S. Atmospheric and environmental effects of the 1783–1784 Laki eruption: A review and reassessment. *J. Geophys. Res.* **108**, 4011 (2003).

118   Ward, P. L. Understanding volcanoes may be the key to controlling global warming. *Soc. Vac. Coaters Bull.* **Summer**, 26-34 (2010).

119   Thordarson, T., Self, S., Oskarsson, N. & Hulsebosch, T. Sulfur, chlorine, and fluorine degassing and atmospheric loading by the 1783–1784 AD Laki (Skaftár Fires) eruption in Iceland. *Bull. Volcanol.* **58**, 205-225 (1996).

120   Licciardi, J. M., Kurz, M. D. & Curtice, J. M. Glacial and volcanic history of Icelandic table mountains from cosmogenic 3He exposure ages. *Quat. Sci. Rev.* **26**, 1529-1546 (2007).

121   Rahmstorf, S. Timing of abrupt climate change: A precise clock. *Geophys. Res. Lett.* **30**, 1510 (2003).

122   Severinghaus, J. P. Abrupt climate change at the end of the last glacial period inferred from trapped air in polar ice. *Science* **286**, 930-934 (1999).

123   Norris, R. D. & Rohl, U. Carbon cycling and chronology of climatewarming during the Palaeocene/Eocene transition. *Nature* **401**, 775-778 (1999).

124   Courtillot, V. E. & Renne, P. R. On the ages of flood basalt events. *C.R. Geosci.* **335**, 113-140 (2003).

125   Wignall, P. The link between large igneous province eruptions and mass extinctions. *Elements* **1**, 293-297 (2005).

126   *Siberian traps*, <en.wikipedia.org/wiki/Siberian_Traps> (2012).

127   Visscher, H. *et al.* Environmental mutagenesis during the end-Permian ecological crisis. *Proc. Nat. Acad. Sci. U.S.A.* **101**, 12952 (2004).

128   Cogné, J.-P. & Humler, E. Trends and rhythms in global seafloor generation rate. *Geochemistry Geophysics Geosystems* **7**, Q03011 (2006).

129   Sigmundsson, F. *et al.* Intrusion triggering of the 2010 Eyjafjallajökull explosive eruption. *Nature* **468**, 426-430 (2010).

130   De Muer, D. & De Backer, H. Revision of 20 years of Dobson total ozone data at Uccle (Belgium): Fictitious Dobson total ozone trends induced by sulfur dioxide trends. *J. Geophys. Res.* **97**, 5921-5937 (1992).

131   Palais, J. & Sigurdsson, H. in *Understanding Climate Change* Vol. 52 (eds A. Berger, R.E. Dickinson, & John W. Kidson) 31-56 (American Geophysical Union Geophysical Monograph, 1989).

132   Freda, C., Baker, D. & Scarlato, P. Sulfur diffusion in basaltic melts. *Geochim. Cosmochim. Acta* **69**, 5061-5069 (2005).

133   Lee, C. T. A., Luffi, P., Plank, T., Dalton, H. & Leeman, W. P. Constraints on the depths and temperatures of basaltic magma generation on Earth and other terrestrial planets using new thermobarometers for mafic magmas. *Earth Planet. Sci. Lett.* **279**, 20-33 (2009).

134   Thorarinsson, S. & Sigvaldason, G. The Hekla eruption of 1970. *Bull. Volcanol.* **36**, 269-288 (1972).

135   Thorarinsson, S. *Hekla: A notorius volcano*. (Almenna Bokafelagid, 1970).

136   Cordero, E., Newman, P. A., Weaver, C. & Fleming, E. *The Brewer-Dobson Circulation*, <www.ccpo.odu.edu/~lizsmith/SEES/ozone/class/Chap_6/index.htm> (2012).